Engineering Structures 32 (2010) 238–249

Contents lists available at ScienceDirect

Engineering Structures

journal homepage: www.elsevier.com/locate/engstruct

Evaluation of the performance of a sliding-type base isolation system with a NiTi shape memory alloy device considering temperature effects

Osman E. Ozbulut, Stefan Hurlebaus *

Zachry Department of Civil Engineering, Texas A&M University, 3136 TAMU College Station, TX 77843, United States

ARTICLE INFO

Article history:
Received 9 June 2009
Received in revised form
5 September 2009
Accepted 8 September 2009
Available online 30 September 2009

Keywords:
Shape memory alloy
Superelasticity
Fuzzy model
Seismic control
Bridges
Earthquake

ABSTRACT

This paper investigates the seismic performance of a sliding-type base isolation system considering environmental temperature changes. The isolation system consists of a steel–Teflon sliding bearing that carries the vertical loads and dissipates energy as a result of its frictional behavior and a shape memory alloy (SMA) device that provides re-centering force and additional damping. A five-span continuous bridge is modeled with sliding bearings and an SMA device as a two-degree-of-freedom system. A neuro-fuzzy model that is capable of capturing the material response at different temperatures and loading frequencies is used to predict the force at superelastic NiTi shape memory alloy wires. The design parameters of the SMA device, i.e., the length and cross-sectional area of NiTi wires, are obtained through a multi-objective genetic algorithm optimization process. A time-domain method that uses wavelet operations for the matching of an accelerogram to the pseudo-acceleration or displacement ordinates for a given design spectrum is employed to generate ground motion records used in the simulations. Finally, nonlinear time history analyses of the isolated bridge are conducted for outside temperatures of 0 °C, 20 °C and 40 °C. The results show that a sliding-type isolation system with an SMA re-centering device can effectively reduce the seismic response of bridges for each temperature considered in the study.

1. Introduction

In past decades, seismic isolation became one of the most commonly used methods for controlling the response of bridge structures. Seismic isolation is essentially based on decoupling of the structure from the supporting ground in order to alleviate the effect of the ground motion on the structure. Various seismic isolation systems have been developed and several have also been applied in practice [1]. Recently, shape memory alloys (SMAs) have attracted much attention as a smart material that can be used in passive protection systems [2].

SMAs have two unique properties: shape memory effect and superelasticity. They owe these unique characteristics to solid-to-solid phase transformations between two stable phases, namely, martensite and austenite. An SMA that is initially in the martensite phase can recover its original shape by heating after experiencing a certain level of stress. This is known as the shape memory effect. If the material is initially in the austenite phase, the shape recovery occurs upon removal of applied loads without heating the material, and this is named as superelasticity (Fig. 1).

A number of researchers have explored the potential applications of superelastic SMAs for vibration control of civil structures. Some researchers have developed SMA-based passive control devices [3–8], some others have proposed energy dissipating braces using SMAs [9–15], while still several other researchers have studied SMA beam–column connections [16–18]. Despite the large number of studies for the application of SMAs in seismic control of civil structures, the number of studies that investigate the potential use of SMAs for seismic protection of bridges is limited. Yet, there are several studies that have been performed to determine applicability of SMAs for bridge structures.

A few researchers have explored the use of SMAs as a restrainer for reducing hinge openings in simply supported bridges [19–21]. In such a study, Johnson et al. [21] conducted large-scale experimental tests on a multiple-span concrete bridge to investigate the performance of SMA restrainer cables. They tested an in-span hinge of a concrete box girder bridge with SMA or traditional steel restrainers and compared the results. Saiidi and Wang [22] proposed the use of shape memory alloys bars as longitudinal reinforcement in plastic hinge regions of reinforced concrete bridge piers. Sharabash and Andrawes [23] studied the performance of cable-stayed bridges that are upgraded with SMA dampers by performing simulations of a 3D finite element bridge model.

The use of SMAs as an isolation system component has also been investigated by some researchers. Seismic isolation systems are typically rubber-based bearings or sliding-type bearings. Rubber isolation bearings have considerable lateral flexibility and lengthen the natural period of the structure in order to avoid resonance with

* Corresponding author. Tel.: +1 979 845 9570; fax: +1 979 845 6554.
E-mail address: shurlebaus@civil.tamu.edu (S. Hurlebaus).

0141-0296/$ – see front matter © 2009 Elsevier Ltd. All rights reserved.
doi:10.1016/j.engstruct.2009.09.010

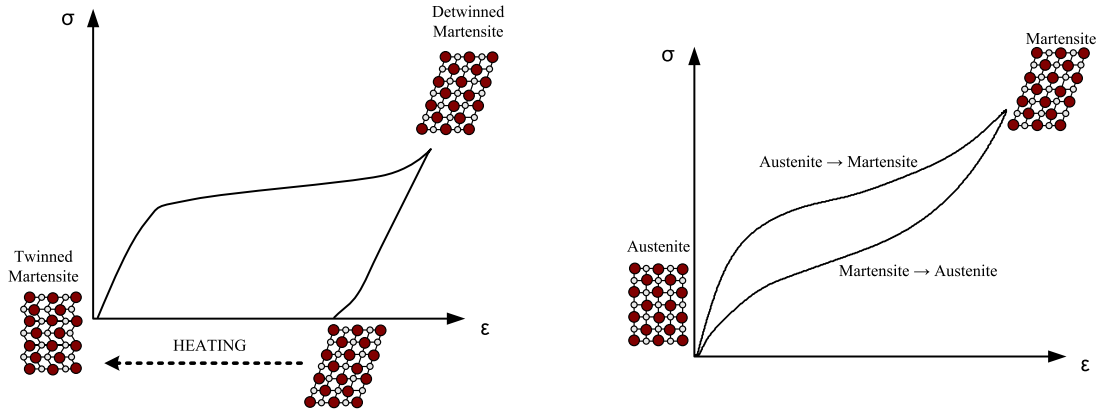

Fig. 1. Shape memory effect and superelasticity.

the predominant frequency contents of the ground motions, while sliding-type bearings provide discontinuous sliding interfaces to separate out lateral forces exerted by an earthquake. In general, a favorable isolation device should have (i) adequate energy dissipation capacity to reduce seismic demand on piers, (ii) a good re-centering mechanism to avoid excessive bearing deformations and instability, (iii) no need for bearing replacement even after a strong earthquake (i.e., no residual deformation on the bearing after the excitation), and (iv) high durability against cyclic loads. SMAs have considerable energy dissipation capacity and re-centering ability that can be exploited for use in a base isolation system. Moreover, superelastic SMAs can fully recover their deformations after an excitation and have substantial resistance to fatigue and corrosion. Because of these appealing properties of SMAs, several researchers suggested an SMA-based seismic isolation device as an alternative system that can accomplish above-mentioned auspicious isolator characteristics.

Wilde et al. [24] proposed a base isolation system that is composed of a laminated rubber bearing and an SMA device. They compared the performance of the proposed isolation system with a laminated rubber bearing that has a lead core. Choi et al. [25] developed a new isolation system for seismic protection of bridges using elastomeric bearings and SMA wires. Analytical studies on a multi-span steel bridge illustrate that the combination of an SMA–rubber bearing effectively decreases relative displacement between deck and pier when compared with a conventional lead–rubber bearing. In another study, Casciati et al. [26] introduced an innovative isolation device in which a sliding system is coupled with inclined CuAlBe shape memory alloy bars that function for energy dissipating and re-centering purposes. However, in these studies, the effect of environmental temperature on the performance of SMA components has not been addressed [27]. In a study in which the temperature effects were considered, Dolce et al. [28] compared the performance of three different sliding-type isolation systems that employ rubber, steel or shape memory alloys as an auxiliary device. They reported a high sensitivity to temperature for an SMA isolation system. In particular, they found variations in peak displacement response up to 103% and in maximum isolator force up to 33% for a ± 30 °C temperature change.

In this study, the seismic performance of a base isolation system consists of a steel–Teflon sliding bearing that decouples superstructure of a bridge from the piers and dissipate energy through friction, and an SMA device that provides restoring force and additional damping capacity is investigated for various outside temperatures. First, a neuro-fuzzy model that captures behavior of NiTi shape memory alloys at different temperatures is introduced. Then, a multi-span continuous bridge is modeled with sliding-type bearings and SMA devices. The temperature effects on steel–Teflon sliding bearings are considered by employing a modified viscoplastic model and using different model parameters for each temperature. An optimization is performed to determine design parameters of the SMA device by using a multi-objective genetic algorithm. In order to generate artificial acceleration records for time history analysis of the isolated bridge, a time-domain method that adjusts historical records for a given design spectrum at multiple damping levels is used. Finally, the structural response of the isolated bridge to various excitation records at different environmental temperatures is studied by conducting nonlinear time history analyses.

2. Modeling superelastic shape memory alloys

The inherent complexity of superelastic behavior of SMAs makes modeling behavior of the material challenging. Many researchers have studied to develop constitutive models that can reproduce complex stress–strain relationship of SMAs [29–32]. However, most of these studies aim to model quasi-static material response and neglect rate- and/or temperature-dependent behavior of SMAs [33]. Since SMAs will be exposed to dynamic effects and temperature changes when they are used for seismic control of bridges, it is important to consider the dependence of the mechanical response of SMAs on the high loading rate and temperature. However, considering the loading rate and/or temperature effects makes SMA constitutive models complicated and numerically expensive to implement into simulations.

In this study, a neuro-fuzzy technique is used to develop a simple, accurate, and computationally efficient model for simulating the superelastic behavior of NiTi shape memory alloys. Here, a brief discussion of the neuro-fuzzy model is given, yet a detailed description of the model can be found in [34].

Fuzzy logic and neural networks are among the soft computing technologies that have been widely used in engineering applications in past decades. The combination of these methods results in intelligent systems that possess the strengths of each technique. The adaptive neuro-fuzzy inference system (ANFIS) is such a hybrid system that allows a fuzzy model to learn its parameters using neural network strategies [35].

The first step in fuzzy modeling is to set up training, checking, and validation data sets for ANFIS simulations. Here, experimental test results on NiTi wires with a diameter of 1.5 mm are used to build the required data sets. The wire is obtained from SAES Smart Materials, and has a 55.8 wt. % nickel with a balance of titanium. The austenite start and finish temperatures are specified by manufacturer as $A_s = -10$ °C and $A_f = 5$ °C, respectively. The uniaxial tensile tests are conducted using an MTS (material testing system) servo-hydraulic load frame in order to characterize dynamic behavior of superelastic SMAs at different temperatures. Specifically,

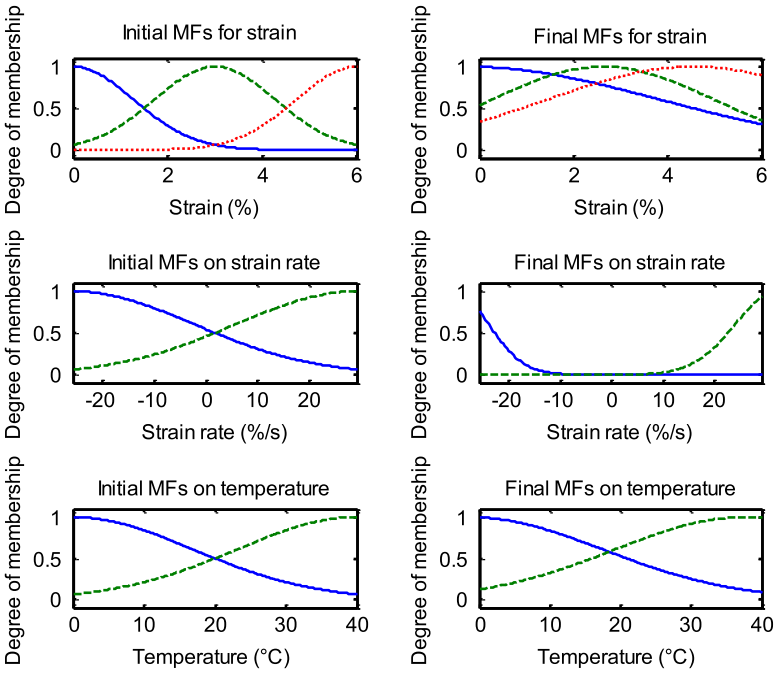

Fig. 2. Initial and final membership function of FIS.

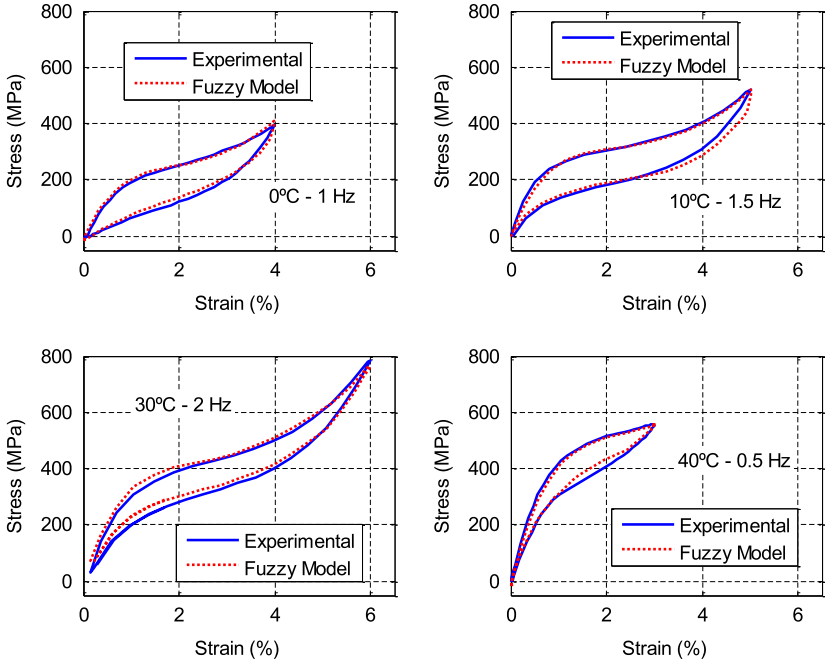

Fig. 3. Model validation: Hysteresis loops at various conditions for experimental results and ANFIS prediction.

the tests are conducted in the temperature range of 0 °C–40 °C for maximum strain amplitudes of 2%–6% while the loading frequency is changed in a range from 0.5 Hz to 2 Hz during the tests.

The test results are concatenated to form the required data sets for ANFIS simulations. Each of training, checking, and validation data sets are composed of 17,090 data points. Then, an initial fuzzy inference system (FIS) with three inputs and a single output is created. The inputs of FIS are selected to be strain, strain rate, and temperature, and the output is the stress on the SMA wire. The strain and stress on the wire are computed directly from measured displacement and force values, and the strain rate is computed by numerical differentiation of strain data. After a trial and error procedure, three Gaussian membership functions are used for strain input, and two Gaussian membership functions are selected for the strain rate and temperature inputs in order to fuzzify each input variable. Also, 12 if-then rules are defined to map the input variables to single output. These initial membership function and rules are randomly generated and need to be tuned in order to predict the correct output that is the stress on SMA wire for given inputs. ANFIS is used to train suitable membership functions and rules based on experimental training and checking data. While training data helps ANFIS to learn about the characteristics of SMA material response, checking data avoid overfitting. Fig. 2 shows the initially defined membership functions for each input, and the adjusted membership functions by ANFIS. As shown from the figure, ANFIS considerably adjusts initial membership functions, especially ones defined for the strain and strain rate, so that they can successfully map the given inputs to the correct output (stress) value.

The final step is to validate the trained FIS with a new set of data that has not been used during training. Fig. 3 illustrates the

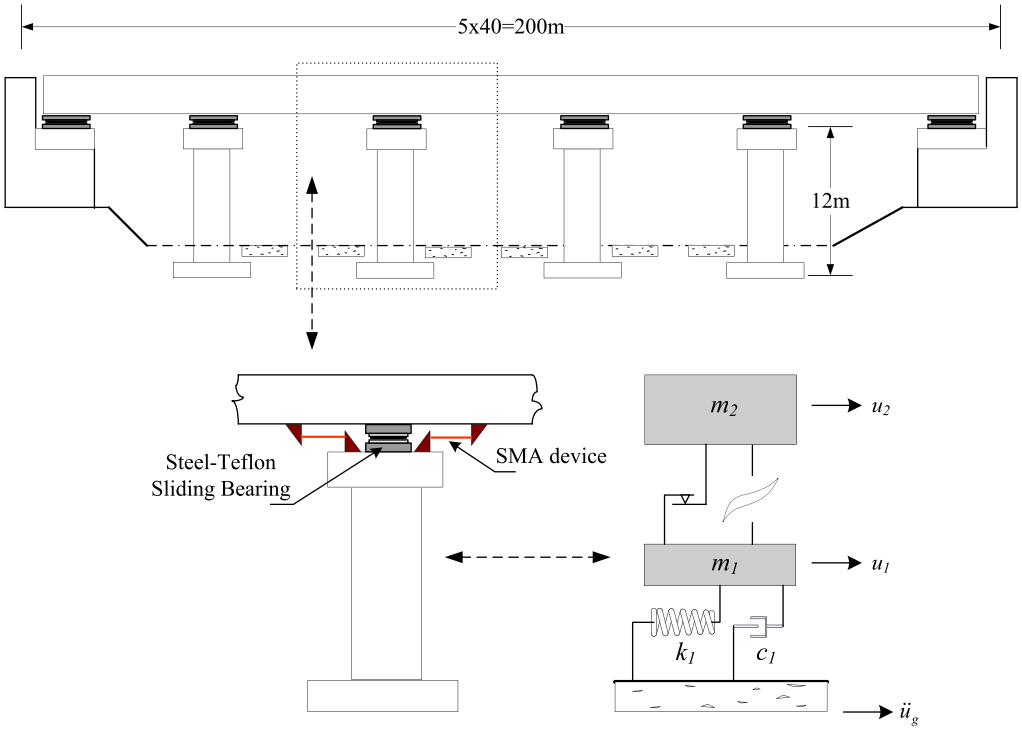

Fig. 4. Five-span continuous bridge and its model with sliding bearings and SMA device.

strain–stress curves plotted for the results of the developed model and experimental tests at various temperatures and loading frequencies as well as at different strain amplitudes. It can be seen from the figure that the developed FIS successfully simulates the behavior of superelastic NiTi wires at different conditions.

3. Analytical study of an isolated bridge

3.1. Modeling of the five-span continuous bridge

The bridge considered in this study has five-span continuous deck with a total length of 200 m and a width of 12 m [36]. Four reinforced concrete columns that have a height of 12 m and two abutments support the superstructure of the bridge. Here, the bridge is isolated using steel–Teflon sliding bearings that utilize an SMA device to provide re-centering force and additional damping. One of the interior spans is selected as an analytical unit and modeled as a two-degree-of-freedom system (Fig. 4). The effective masses of deck and column are given as 600 and 243.15 ton, respectively. The columns are assumed to be perfect elastoplastic with an initial stiffness of 112 700 kN/m and yield displacement of 0.0309 m. Also, 2% viscous damping is assumed for the piers.

The equations of motion are

$$\begin{aligned} m_1\ddot{u}_1 + F_p - F_{IS} &= -m_1\ddot{u}_g \\ m_2\ddot{u}_2 + F_{IS} &= -m_2\ddot{u}_g, \end{aligned} \tag{1}$$

where m_1, m_2 and u_1, u_2 are the masses and displacements of pier and deck, respectively, and $\ddot{u}_g$ is the ground acceleration. F_p represents nonlinear pier force and computed as

$$\begin{aligned} F_p &= \alpha k_1 u_1 + (1-\alpha)k_1 u_y z + c_1\dot{u}_1 \\ u_y\dot{z} &+ \gamma\,|\dot{u}_1|\,|z|\,|z|^{n-1} + \beta\dot{u}_1\,|z|^n - \dot{u}_1 = 0 \end{aligned} \tag{2}$$

where α is the ratio of the post yielding to the elastic stiffness, u_y is the yield displacement of piers, and z is the hysteretic Bouc–Wen quantity governed by the above differential equation and the dimensionless parameters γ, β and n are taken as 0.5, 0.5, and 1, respectively. F_{IS} denotes restoring force of isolation systems. Hence, F_{IS} is the sum of the nonlinear force of the SMA device and frictional resistance force of steel–Teflon sliding bearings.

In order to analyze the dynamic response of structures with sliding systems, two different numerical models, namely conventional friction and continuous hysteretic models, are mainly used by researchers in the past. In the conventional model, the frictional force of the isolation system is evaluated by solving different set of equations for sliding and non-sliding phases [37]. On the other hand, the hysteretic model is a continuous model, and the frictional force can be obtained from a modified viscoplastic model developed by Constantinou et al. [38]. Although in terms of computational efficiency and applicability to the general computer code two models are found to have relative advantages and disadvantages, it is also observed that both models predict the seismic response of sliding isolation systems similarly [39]. Here, the hysteretic model is used to simulate the force of the sliding bearings. The frictional force at a sliding interface is given by

$$F_f = \mu_s W Z \tag{3}$$

where μ_s represents the coefficient of friction, W is the normal load carried by the bearing interface, and Z is a hysteretic dimensionless quantity computed from following equation

$$Y\dot{Z} + \gamma\,|\dot{u}_b|\,|Z|\,|Z|^{n-1} + \beta\dot{u}_b\,|Z|^n - \dot{u}_b = 0, \tag{4}$$

where Y is the yield displacement of the sliding bearing chosen as 0.0005 m and, γ, β, and n are dimensionless parameters that control the shape of the hysteretic curve and have the values of 0.9, 0.1 and 1, respectively. Also, $u_b = u_2 - u_1$ is the deformation of the sliding bearings.

Experimental studies showed that the coefficient of friction of steel–Teflon sliding bearings tends to decrease with increasing stress and increase with increasing velocity. It may be approximated at sliding velocity $\dot{u}_b$ as

$$\mu_s = \mu_{\max} - \Delta\mu\,\exp\left(-a\,|\dot{u}_b|\right), \tag{5}$$

where $\mu_{\max}$ is the coefficient of friction at very high velocities, and $\Delta\mu$ is the difference between the coefficient of friction at

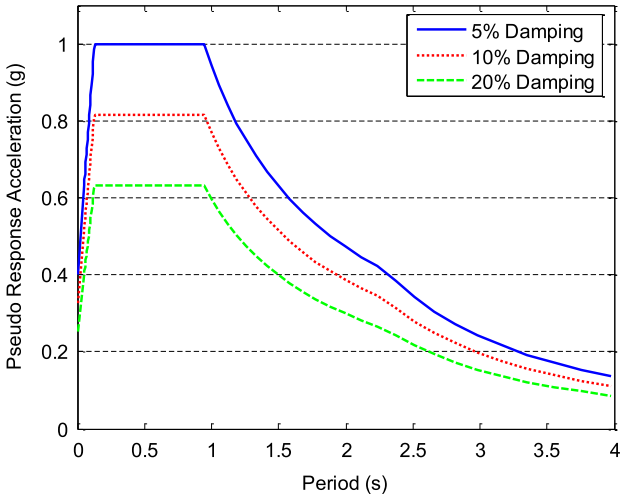

Fig. 5. Target spectrum at different damping levels.

Table 1
Model parameters for different temperatures.

T (°C)	μ_{max} (%)	$\Delta\mu$ (%)	a(m/s)
0	11.07	6.78	23.3
20	10.26	7.13	22
40	9.86	7.11	18.7

very high and very low velocities. Furthermore, a is a constant for a given bearing pressure and condition of sliding interface. Dolce et al. [40] studied the frictional behavior of steel–Teflon sliding bearings, and specified the parameters μ_{max}, $\Delta\mu$, and a for different combination of bearing pressure, condition of interface and temperature. The temperatures considered in their study are −10 °C, 20 °C, and 50 °C, and the above-mentioned model parameters are specified for these temperatures. Here, a linear interpolation is made to approximate the corresponding parameters for 0 °C, 20 °C, and 40 °C. The values of μ_{max}, $\Delta\mu$, and a for three different temperatures and for a 28.1 MPa bearing pressure and non-lubricated bearing interface are given in Table 1.

The fuzzy model described earlier is used to predict the instantaneous force from the SMA elements at different temperatures. Since design parameters of the SMA device, i.e., the length and cross-sectional area of NiTi wires, depend on the design earthquake intensity level, the ground motions that are considered in this study are described first. Then, a genetic algorithm-based multi-objective optimization method is introduced for the selection of design parameters of SMA wires.

3.2. Input ground motion records

Recorded acceleration time histories of historical earthquakes are usually used as a seismic input in linear and nonlinear dynamic analyses. Although using real strong-motion accelerograms is attractive, it mostly requires scaling of the real record for compatibility with the design response spectrum. However, scaling a single ground motion in frequency domain to match a target design spectrum may totally distort the energy characteristics of accelerograms and produce very unrealistic seismic demands [41].

An alternative approach for generating accelerograms for dynamic analysis has been proposed by Hancock et al. [42]. The method, known as RspMatch2005, modifies a historical accelerogram in time domain by employing wavelet adjustments to match a target design spectrum. One of the advantages of RspMatch2005 is that it does not cause a drift in the velocity or displacement time histories while that is the case for spectral matching in the frequency domain, which causes the unrealistic high-energy content.

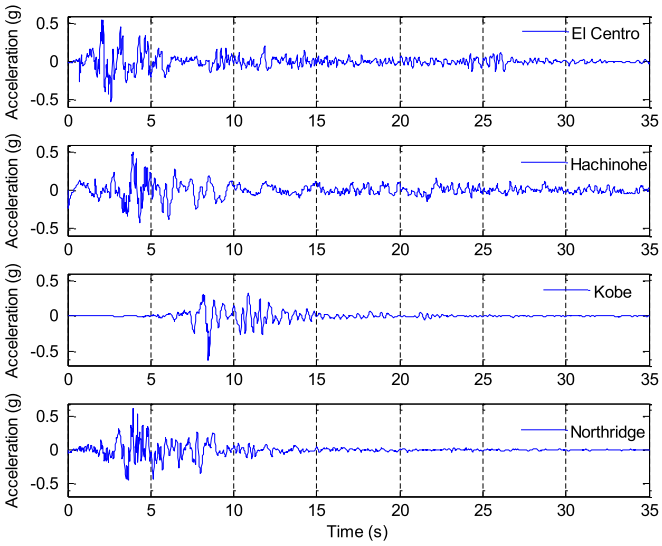

Fig. 6. Spectrally matched acceleration time histories used in simulations.

Also, it enables the accelerogram to be matched to a given target spectrum with several different levels of damping simultaneously, which is useful particularly in the analysis of isolated bridges. Furthermore, in another work of Hancock et al. [43], it is shown that the number of records required to achieve a robust estimate of inelastic response may be significantly reduced through the use of the spectrally matched, wavelet-adjusted accelerograms. Therefore, in this study, RspMatch2005 is employed to obtain historical accelerograms that are spectrally matched to a given spectrum at multiple damping levels for use in time-history analyses.

The target response spectrum is constructed using the AASHTO LRFD bridge design specifications [44] for site class B with peak ground acceleration of 0.40 g and is shown for damping levels of 5%, 10% and 20% in Fig. 5. In order to start the RspMatch2005 process, a suite of initial accelerograms that may be linearly scaled to have an approximate match to the spectral shape of the 5% damped target spectrum is needed. Seven historical earthquake records (1940 El Centro, 1968 Hachinohe, 1986 North Palm Spring, 1994 Northridge, 1995 Kobe, 1999 Chi-Chi, and 1999 Bolu) are considered for initial selection, and their match with the target spectrum is assessed using the root mean square (RMS) difference between the normalized spectral acceleration of observed and target spectra (ΔSAn_{RMS}) which is given as [42]

$$\Delta SAn_{RMS} = \sqrt{\frac{1}{N_p}\sum_{i=1}^{N_p}\left(\frac{PSA_0(T_i)}{PGA_0} - \frac{PSA_s(T_i)}{PGA_s}\right)^2}, \quad (6)$$

where N_p is the number of periods, $PSA_0(T_i)$ is the pseudo spectral acceleration from the record at period T_i, $PSA_s(T_i)$ is the target pseudo spectral acceleration at the same period; PGA_0 and PGA_s are the peak ground acceleration of the accelerogram and zero-period anchor point of the target spectrum. After comparing ΔSAn_{RMS} of seven ground motions, 1940 El Centro, 1968 Hachinohe, 1994 Northridge, and 1995 Kobe records are selected as seed accelerograms due to better match of their spectral shape.

The selected seed accelerograms are matched to the target spectra at multiple damping levels using RspMatch2005. Fig. 6 illustrates adjusted acceleration time-histories for El Centro, Hachinohe, Kobe, and Northridge earthquakes. Fig. 7 shows original, target, and adjusted response spectra of Northridge ground motion. The original response spectrum is given for 5% damping while target and adjusted spectra is plotted for 5, 10, and 20% damping levels. It can be seen that there is no exact match for all three damping levels, but spectral misfit at all damping spectra of

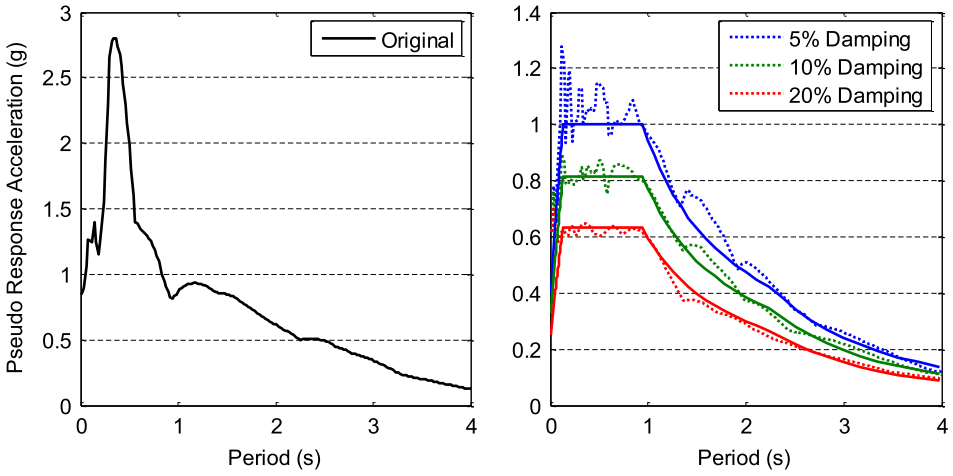

Fig. 7. Original and adjusted response spectra to simultaneously match the 5%, 10%, and 20% damped target spectra for Northridge earthquake.

the record is largely decreased. The acceleration records shown in Fig. 6 are used as a seismic input in the time history analyses of the isolated bridge that is discussed in the next section.

3.3. Design of SMA device

Although the cost of SMA material has decreased significantly in the past decade [45], it has been one of the impediments to actual implementation. Yet, economically feasible solutions can be attained with NiTi-based SMAs if they are used in small devices or applied to a selected region of structures [46]. The SMA device considered in this study has a straightforward design, which avoids extra fabrication costs. It simply consists of multiple loops of superelastic NiTi wires wrapped around two wheels.

In order to choose design parameters of SMA re-centering damping device, a trial and error is usually required. It is possible to alter the nonlinear stiffness and damping added to the system by changing the geometry of SMA elements. One of the main concerns in design is to keep the maximum strain of SMA wires during strongest motion within the recovarable superelastic strain range (up to 6%–7% for NiTi wires) of the material. That requires long wire length. Also, the cross-sectional area of the SMA wires should be large enough to develop the required re-centering force for the isolation system. Yet, other objectives in design are to limit the shear force transferred to the piers and minimize the total volume of the material that is used for the device.

In this study, a multi-objective genetic algorithm optimizer, namely NSGA-II, is used in order to determine the optimum length and area of NiTi wires. NSGA-II is a computationally fast and elitist evolutionary algorithm based on a non-dominated sorting approach. Among a pool of initial random candidate values that reside within a user-defined range, NSGA-II generates a set of Pareto-optimal solutions through an iterative process. The detailed description of NSGA-II algorithm can be found in [47,48]. Here, three objective functions, namely, peak deck relative displacement, peak deck acceleration, and peak base shear, are considered. All three have to be minimized simultaneously. In order to avoid training with several historical ground motions during the optimization process, spectrally matched Northridge accelerogram is used as a seismic input. A population of size 50 is selected and each simulation is run for 100 generations. In order to discourage Pareto-optimal solutions that cause SMA wires to experience more than 6% strain, a fixed large penalty is added to all objectives if the maximum strain of the wires is over 6%. The optimization is devised for an outside temperature of 0 °C since it is observed that SMA wires are exposed to larger strains at this temperature during preliminary investigations. The results of genetic algorithm optimization reveal that selecting a wire length of 2.35 m and a cross-sectional area of 620 mm^2 that corresponds to 350 NiTi wires with a diameter of 1.5 mm for each SMA device gives optimal solution. Therefore, these values are used for an SMA device in numerical simulations described below.

4. Results

Nonlinear equations of motion given above in Eq. (1) are solved using a fourth-order Runge–Kutta method with variable time step. The response time histories of the isolated bridge equipped with SMA devices are obtained against artificial ground motions described above for different environmental temperatures. In this section, first the results for all excitation cases are summarized, and then displacement and acceleration time histories as well as hysteretic force–displacement curves of isolation system components for the Northridge earthquake case are presented.

Fig. 8 demonstrates the results for maximum drifts of the pier and deck at 0 °C, 20 °C, and 40 °C for the considered excitations. It can be seen that the maximum pier displacement usually increases with decreasing environmental temperature. The maximum change in peak pier displacement is +10% and −11% when temperature increases or decreases 20 °C from reference temperature of 20 °C, respectively. The peak relative displacement of deck has its maximum value at 40 °C for all the excitation cases except Kobe earthquake. One reason of this increase in deck drift at higher temperatures is the lower coefficient of friction of sliding bearings at these temperatures. Since the large portion of energy dissipation is provided by frictional behavior of sliding bearings for the isolation system, the decrease in the friction coefficient at higher temperatures results in an increase in the deck displacement response. However, the larger frictional force at low temperatures increases the demand on the piers and cause larger pier drift. The maximum variation of the peak deck drift as temperature changes ±20 °C compared to reference temperature is about 13% which is observed for El Centro earthquake.

Fig. 9 shows the residual pier drift ratio and residual isolation deformation at different temperatures for the considered ground motions. As mentioned above, since the frictional force transferred to piers is larger at low temperatures and SMA re-centering force reduces with decreasing temperature, larger residual pier drift ratios are observed at 0 °C for the all cases except Hachinohe excitation. However, the largest residual pier drift ratio is about 0.12% for Northridge record while it is below 0.06% for the other ground motions. Also, steel–Teflon sliding bearings with an SMA device recover almost all deformations for most of the cases. The

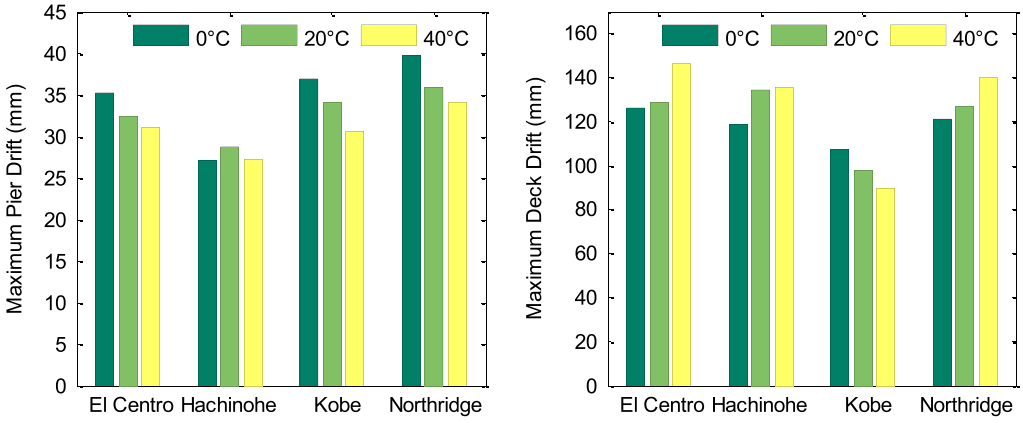

Fig. 8. Maximum drifts of pier and deck at different temperatures.

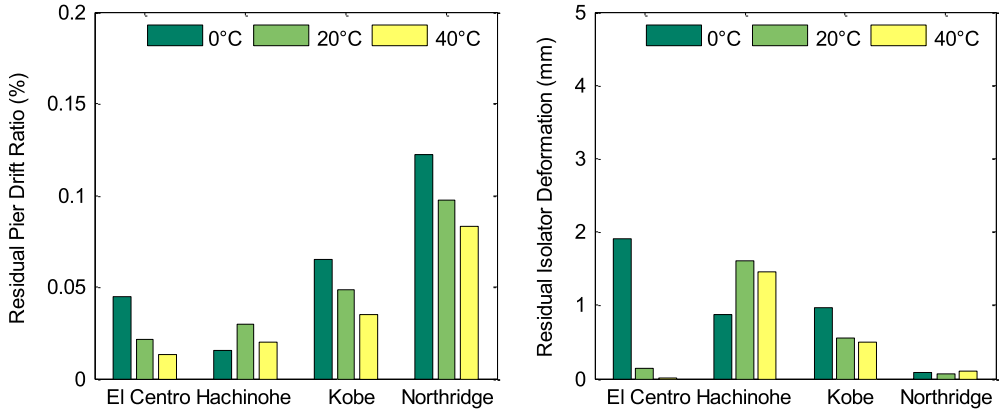

Fig. 9. Residual pier drift ratio and residual deformation of the isolator at different temperatures.

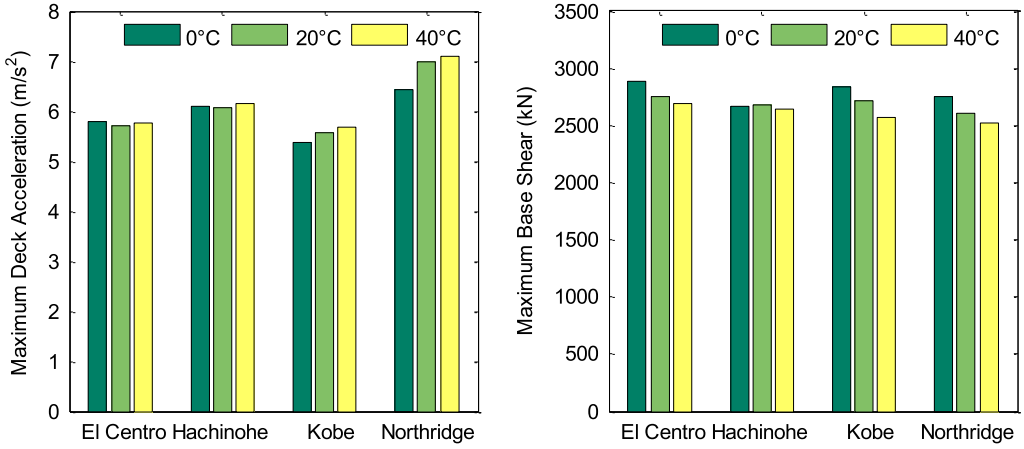

Fig. 10. Maximum deck acceleration and maximum base shear at different temperatures.

largest residual deformation observed for El Centro excitation at 0 °C is about 2 mm.

The variations of the maximum deck acceleration and the maximum base shear with temperature are given in Fig. 10. It can be seen that there is no significant change in peak deck acceleration with the environmental temperature change. In particular, the maximum change in peak deck acceleration is about 1% for El Centro and Hachinohe excitations, while it is about −4% and −8% for Kobe and Northridge, respectively, when temperature decreases to 0 °C from reference temperature of 20 °C. The slight increase in deck acceleration for Kobe and Northridge excitations with the increasing temperature can be attributed to the larger SMA re-centering forces at high temperatures. The maximum base shear experiences a highest of 6% increase for the Northridge record if temperature drops to 0 °C, and it reduces a maximum of 6% for Kobe excitation if temperature increases to 40 °C compared to reference temperature.

The time histories of relative deck displacement and absolute deck acceleration are illustrated in Fig. 11 for lowest and highest outside temperatures (0 °C and 40 °C) considered here for Northridge excitation. As discussed above, the acceleration response of the deck is very similar at both temperatures, whereas the maximum relative displacement of deck is slightly lower at 0 °C.

Fig. 12 shows the force–displacement relationships of the isolation system components, i.e., sliding bearing (SB) and SMA device

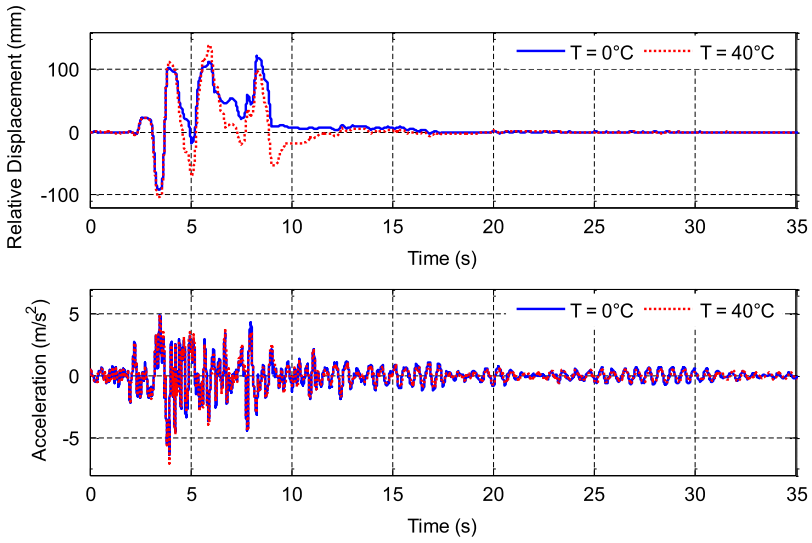

Fig. 11. Time histories of deck relative displacement and deck acceleration at 0 °C and 40 °C.

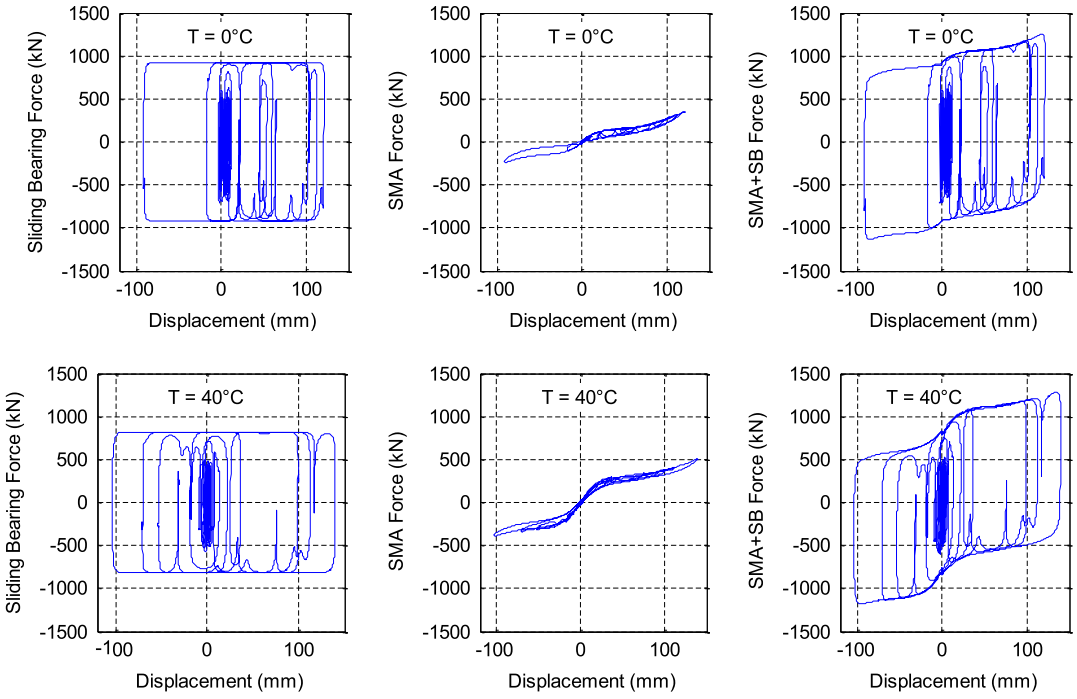

Fig. 12. Hysteresis curves of the isolation system and its components at 0 °C and 40 °C.

together with the combined hysteresis curve at 0 °C and 40 °C during Northridge excitation. It can be seen that re-centering ability of the isolation system improves with increasing temperature while the maximum frictional force, i.e., energy damping capacity of the system decreases. Also, note that the isolation system mainly dissipates the energy through friction while very modest contribution is available from hysteretic behavior of superelastic SMAs.

Fig. 13 compares the maximum forces of sliding bearings, SMA device and combined isolation system for different temperatures. Also, hysteresis loops of the SMA device are given for each temperature in the figure. It can be seen that maximum friction force of steel–Teflon bearings decreases with an increase in temperature due to the lower friction coefficient at higher temperatures. On the other hand, the re-centering force of the SMA device increases with the temperature. Note that the maximum force generated in the SMA device at 0 °C and 20 °C is almost the same. That is because of significant strain hardening of SMA wires at 0 °C for large deformations. Therefore, the maximum SMA force at 0 °C reaches to the maximum force level observed at 20 °C. However, as it can be seen from SMA hysteresis curves, the SMA device has a higher stiffness and generates larger re-centering forces at higher temperatures. If the variation of the combined isolation system force with temperature is examined, it can be seen that it remains more stable since the difference in the forces generated on sliding bearing and SMA device offset each other. Nevertheless, it is apparent that the stiffness of the isolation system increases and the damping capacity of the isolation system decreases with increasing temperature.

In order to assess whether the seismic response of a bridge isolated by SMA-based sliding bearings is more sensitive to the

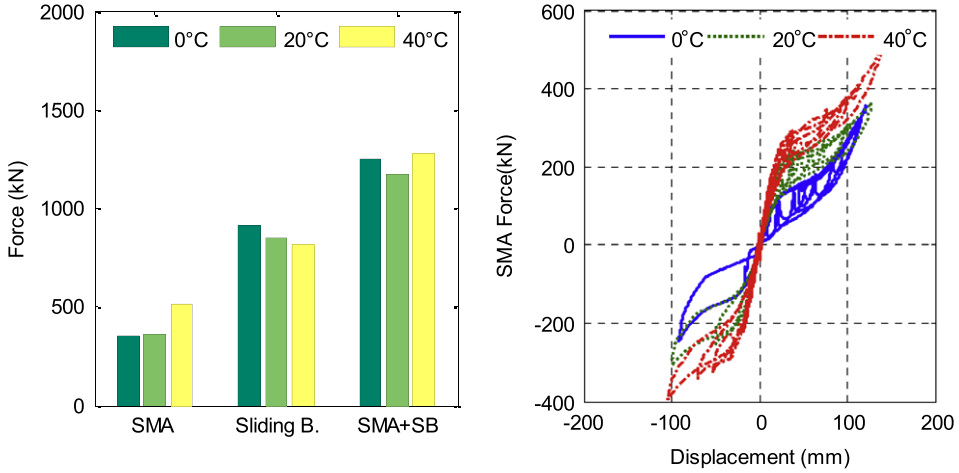

Fig. 13. The variation of maximum forces of the isolation system and its components with temperature and hysteresis loops of SMA device at various temperatures.

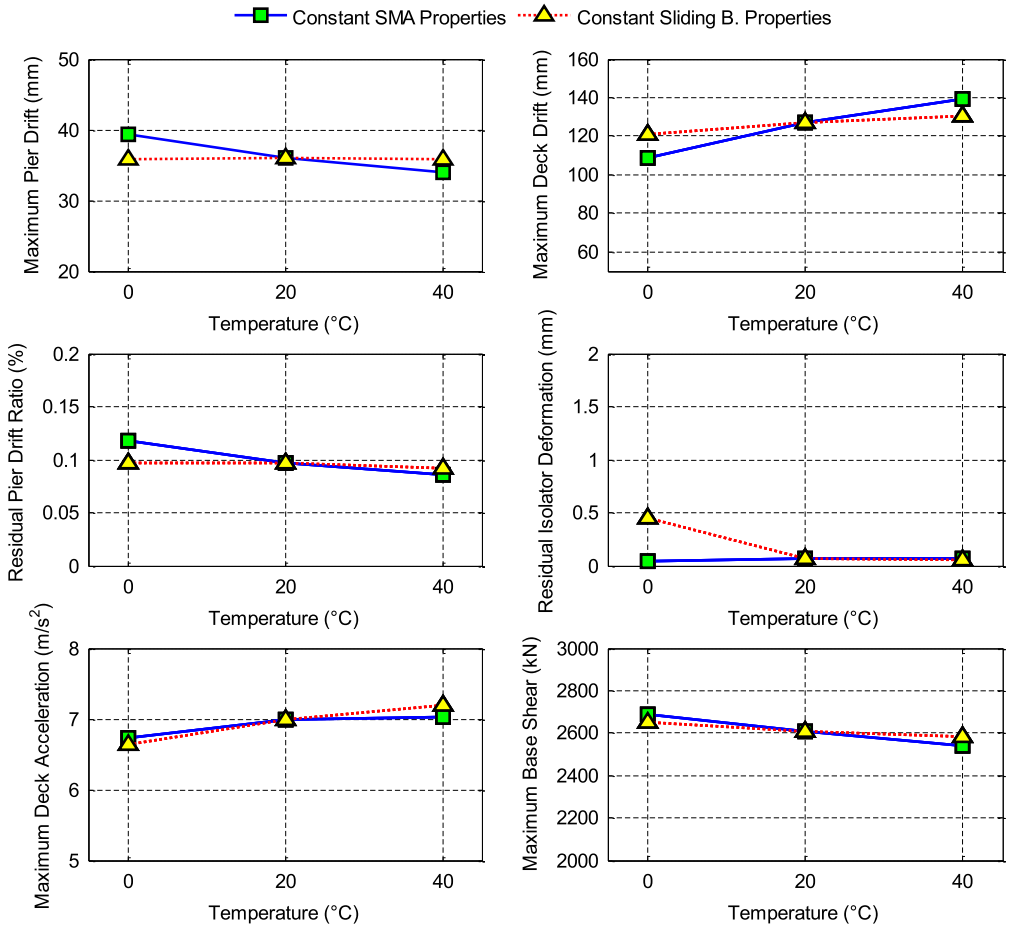

Fig. 14. The variation of the seismic response of the bridge with temperature for constant SMA properties and constant sliding bearing properties.

temperature-dependent properties of sliding bearings or those of SMAs, another set of simulations are performed. First, temperature dependence of SMA behavior is neglected and SMAs wires are modeled for an environmental temperature of 20 °C, while sliding bearing properties are changed for each temperature. Then, the properties of sliding bearings are assumed to be constant and equal to those of at 20 °C, whereas variation of SMA material response with outside temperature is considered. The spectrally matched Northridge earthquake is used as an external excitation. The results are summarized in Fig. 14. It can be seen that the temperature dependence of frictional properties of sliding bearing is contributing more to the variation of the seismic response of the isolated bridge. In particular, the higher frictional force of the bearing at low temperatures results in an increase in the pier drift, and a reduction in deck relative displacement due to larger energy dissipation. Although, the change of SMA properties with changes in temperature also affects the results, the variation of the seismic response of the bridge is more modest for this case. For instance, as temperature changes ±20 °C compared to reference temperature, there is only 5% change in the peak deck drift if the SMA properties changes with the temperature while sliding bearing properties are kept constant. However, the same change is 14% for the case

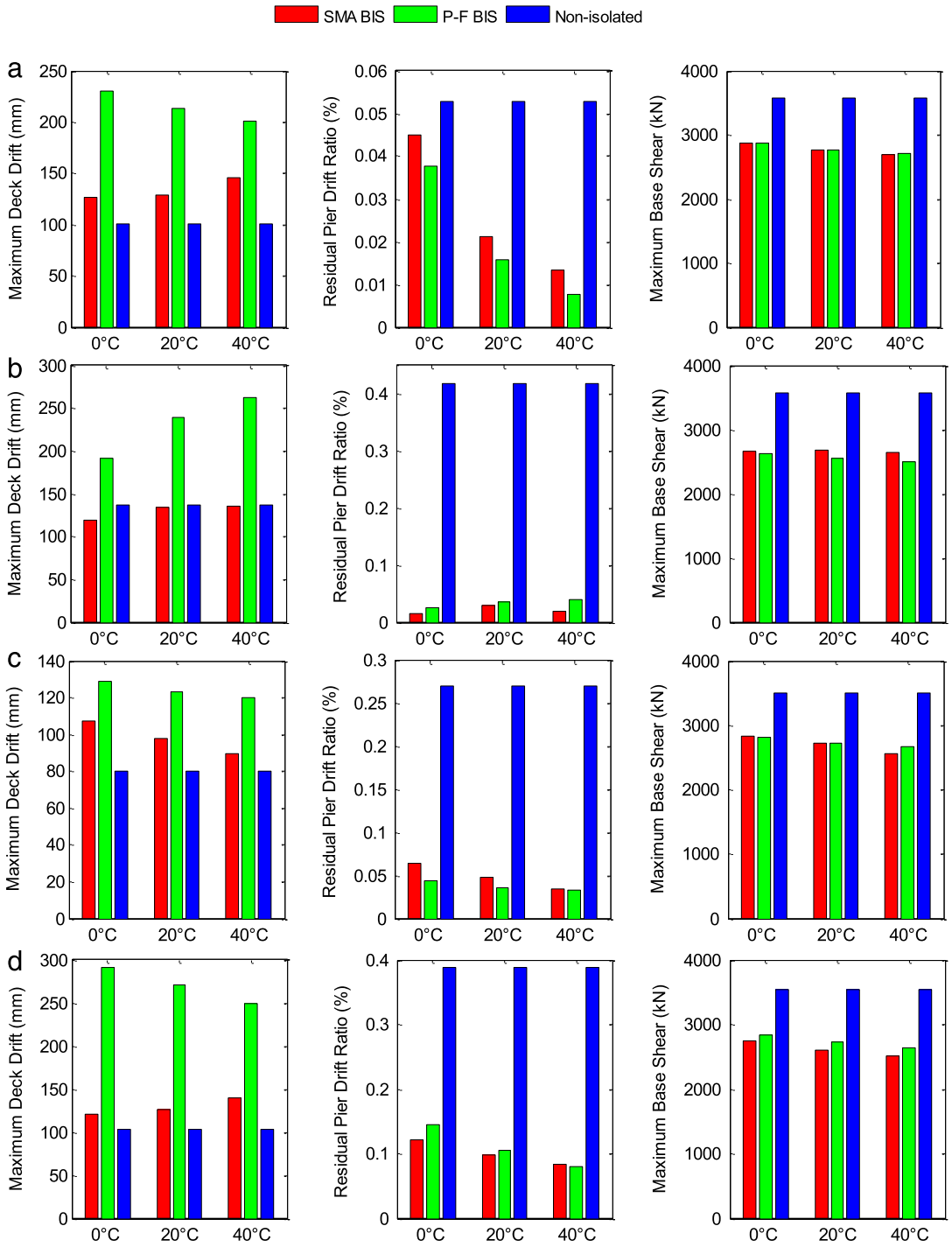

Fig. 15. Seismic response comparison of different bridge configurations at various temperatures for (a) El Centro, (b) Hachinohe, (c) Kobe and (d) Northridge earthquakes.

of constant SMA material behavior and temperature-dependent bearing properties. Also, note that for all cases SMA-based sliding bearings have no residual deformations at the end of ground motion.

Finally, to evaluate the effectiveness of the SMA-based sliding base isolation system (BIS), the seismic performance of the SMA-based sliding BIS is compared with two benchmark cases: (i) the seismic response of the bridge incorporating only the pure-friction (P-F) BIS (i.e. sliding-type bearings without SMA devices) and (ii) the seismic response of the bridge incorporating a monolithic connection between the deck and the top of the piers (i.e. non-isolated bridge). Nonlinear time-history analyses are performed for the temperature range considered in this study and ground motions described above.

Fig. 15 shows the maximum deck drift, residual pier drift ratio and maximum base shear for the bridge isolated by SMA-based sliding isolators and P-F sliding isolators and non-isolated bridge for different ground motions. Also, the results are presented for outside temperatures of 0 °C, 20 °C, and 40 °C. Note that the response for the isolated bridge cases varies with temperature while the results for the non-isolated bridge are constant for each temperature. As shown in the figure, the use of SMA-based sliding isolators decreases the seismic demand on the piers while simultaneously reducing the displacement demand of isolators.

Note that although the bridge isolated by P-F sliding bearings also decreases the demand on the substructure, it has larger deck drifts as compared to SMA-based sliding isolators. Also, large residual isolator deformations are observed for the P-F isolation system after the seismic motion due to the lack of re-centering force capability while the SMA-based sliding isolation system recovers almost all of its deformations as illustrated above in Fig. 9.

5. Conclusion

In this paper, the seismic performance of a sliding-type base isolation system equipped with a NiTi shape memory alloy device is evaluated considering that effects of outside temperature changes for a multi-span continuous bridge. Since the temperature and loading-rate significantly affect the behavior of superelastic NiTi wires, a neuro-fuzzy model that captures material response considering the temperature and strain rate effects is first introduced. The temperature effects on steel–Teflon sliding bearings are considered by using a continuous hysteretic model with different model parameters for each temperature. The length and cross-sectional area of the SMA device is optimized by employing a non-dominated sorting genetic algorithm. The program RspMatch2005, which enables the historical accelerograms to be matched to a given target response spectrum at multiple different levels of damping, is used to obtain a suite of accelerograms for use in dynamic nonlinear analyses of the bridge.

Nonlinear time history analyses of the isolated bridge are conducted for three different outside temperatures. The results show that the temperature has modest effect on the performance of bridges isolated using steel–Teflon sliding bearings with SMA re-centering device. Specifically, there is a maximum of 13% difference on the displacement response of the bridges for all considered ground motions when temperature differs ± 20 °C from the reference temperature of 20 °C. Similarly, the acceleration response of the bridge varies a maximum of 8% with the temperature change while the difference is below 2% for most of the cases. Also, it is noted that the change in the forces generated in sliding bearings and SMA device counterbalance each other. While temperature increases, the frictional force of sliding bearings reduces, i.e., the damping capacity of isolation system decreases. On the other hand, the initial stiffness and yield strength of the SMA device increases with increasing temperature. Therefore, a larger re-centering force is available for high temperatures. Overall, the sliding-type isolation system with the SMA device appears to effectively limit the response of the bridges subjected to earthquake ground motions. Also, it is observed that SMA-based sliding isolators recover almost all of their deformations, which eliminates the need of bearing replacement after a strong earthquake. However, note that NiTi shape memory alloys used in this study completely loose their superelasticity below -10 °C; therefore, the results cannot be generalized for the regions with severe winter conditions. This drawback might be eliminated in the future by the development of NiTi-based superelastic SMAs with a larger operating temperature range, which is a widespread research area.

References

[1] Komodromos P. Seismic isolation for earthquake resistant structures. London: WIT Press; 2000.

[2] Hurlebaus S, Gaul L. Smart structure dynamics. Mech Syst Signal Process 2006; 20:255–81.

[3] Zuo XB, Li AQ, Chen QF. Design and analysis of a superelastic SMA damper. J Intell Mater Syst Struct 2008;19:631–9.

[4] Zhang Y, Zhu S. A shape memory alloy-based reusable hysteretic damper for seismic hazard mitigation. Smart Mater Struct 2007;16:1603–13.

[5] Li H, Mao CX, Qu JP. Experimental and theoretical study on two types of shape memory alloy devices. Earthq Eng Struct Dyn 2008;37:407–26.

[6] Lindt JW, Potts A. Shake table testing of a superelastic shape memory alloy response modification device in a wood shearwall. J Struct Eng 2008;134(8): 1343–52.

[7] Dolce M, Cardone D. Theoretical and experimental studies for the application of shape memory alloys in civil engineering. J Eng Mater Technol 2006;128: 302–11.

[8] Ma H, Cho C. Feasibility study on a superelastic SMA damper with re-centering capability. Mater Sci Eng A 2006;473:290–6.

[9] Torra V, Isalgue A, Martorell F, Terriault P, Lovey FC. Built in dampers for family homes via SMA: An ANSYS computation scheme based on mesoscopic and microscopic experimental analyses. Eng Struct 2007;29(8):1889–902.

[10] Salich J, Hou Z, Noori M. Vibration suppression of structures using passive shape memory alloy energy dissipation devices. J Intell Mater Syst Struct 2001; 12:671–80.

[11] Lafortune P, McCormick J, DesRoches R, Terriault P. Testing of superelastic recentering pre-strained braces for seismic resistant design. J Earthq Eng 2007; 11:383–99.

[12] Motahari SA, Ghassemieh M, Abolmaali SA. Implementation of shape memory alloy dampers for passive control of structures subjected to seismic excitations. J Constr Steel Res 2007;63:1570–9.

[13] McCormick J, DesRoches R, Fugazza D, Auricchio F. Seismic vibration control using superelastic shape memory alloys. J Eng Mater Technol 2006;128: 294–301.

[14] Boroschek RL, Farias G, Moroni O, Sarrazin M. Effect of SMA braces in a steel frame building. J Earthq Eng 2007;11:326–42.

[15] Bartera F, Giacchetti R. Steel dissipating braces for upgrading existing building frames. J Constr Steel Res 2004;60:751–69.

[16] Ocel J, DesRoches R, Leon RT, Hess G, Krummes R, Hayes JR, Sweeney S. Steel beam–column connections using shape memory alloys. J Struct Eng 2004; 130(5):732–40.

[17] Sepulveda J, Boroschek R, Herrera R, Moroni O, Sarrazin M. Steel beam–column connection using copper-based shape memory alloy dampers. J Constr Steel Res 2008;429:35.

[18] Penar BW. Recentering beam–column connections using shape memory alloys. Masters' thesis. School of Civil and Environmental Engineering, Georgia Institute of Technology; 2005.

[19] Andrawes B, DesRoches R. Unseating prevention for multiple frame bridges using superelastic devices. Smart Mater Struct 2005;14:60–7.

[20] DesRoches R, Delemont M. Seismic retrofit of simply supported bridges using shape memory alloys. Eng Struct 2002;24(3):325–32.

[21] Johnson R, Padgett JE, Maragakis ME, DesRoches R, Saiidi MS. Large scale testing of nitinol shape memory alloy devices for retrofitting of bridges. Smart Mater Struct 2008;17:1–10.

[22] Saiidi M, Wang H. Exploratory study of seismic response of concrete columns with shape memory alloys reinforcement. ACI Struct J 2006;103:436–43.

[23] Sharabash AM, Andrawes BO. Application of shape memory alloy dampers in the seismic control of cable-stayed bridges. Eng Struct 2009;31:607–16.

[24] Wilde K, Gardoni P, Fujino Y. Base isolation system with shape memory alloy device for elevated highway bridges. Eng Struct 2000;22:222–9.

[25] Choi E, Nam TH, Oh JT, Cho BS. An isolation bearing for highway bridges using shape memory alloys. Mater Sci Eng A 2006;438–440:1081–4.

[26] Casciati F, Faravelli L, Hamdaoui K. Performance of a base isolator with shape memory alloy bars. Earthq Eng Eng Vib 2007;6(4):401–8.

[27] Zhang Y, Camilleri JA, Zhu S. Mechanical properties of superelastic Cu-Al-Be wires at cold temperatures for the seismic protection of bridges. Smart Mater Struct 2008;17:1–9.

[28] Dolce M, Cardone D, Palermo G. Seismic isolation of bridges using isolation systems based on flat sliding bearings. Bull Earthq Eng 2007;5:491–509.

[29] Muller I, Seelecke S. Thermodynamic aspects of shape memory alloys. Math Comput Modelling 2001;34(12–13):1307–55.

[30] Liang C, Rogers CA. One-dimensional thermo mechanical constitutive relations for shape memory material. J Intell Mater Syst Struct 1990;1:207–34.

[31] Brinson LC. One-dimensional constitutive behavior of shape memory alloys: thermomechanical derivation with non-constant material functions and redefined martensite internal variable. J Intell Mater Syst Struct 1993;4: 229–41.

[32] Boyd JG, Lagoudas DC. Thermodynamical constitutive model for shape memory materials. Part I. The monolithic shape memory alloy. Int J Plasticity 1996;12(6):805–42.

[33] Motahari SA, Ghassemieh M. Multilinear one-dimensional shape memory material model for use in structural engineering applications. Eng Struct 2007; 29:904–13.

[34] Ozbulut OE, Hurlebaus S. A temperature- and strain-rate-dependent model of NiTi shape memory alloys for seismic control of bridges. In: Sensors and smart structures technologies for civil, mechanical, and aerospace systems. Proceedings of SPIE 2009;7292, 729241.

[35] Jang JR, Sun C, Mizutani E. Neuro-fuzzy and soft computing: a computational approach to learning and machine intelligence. Upper Saddle River: Prentice Hall; 1997.

[36] Lee TY, Kawashima K. Semiactive control of nonlinear isolated bridges with time delay. J Struct Eng 2007;133(2):235–41.

[37] Bozzo L, Barbat AH. Non-linear response of structures with sliding base isolation. J Struct Control 1995;2:59–77.

[38] Constantinou M, Mokha A, Reinhorn A. Teflon bearing in base isolation II: Modeling. J Struct Eng 1990;116(2):455–74.

[39] Jangid RS. Computational numerical models for seismic response of structures isolated by sliding sytems. Struct Control Health Monitor 2005;12:117–37.
[40] Dolce M, Cardone D, Croatto F. Frictional behavior of Steel-PTFE interfaces for seismic isolation. Bull Earthq Eng 2005;3:75–99.
[41] Naeim F, Kelly JM. Design of isolated structures. New York: John Wiley & Sons; 1999.
[42] Hancock J, Watson-Lamprey J, Abrahamson NA, Bommer JJ, Markatis A, McCoy E, Mendis R. An improved method of matching response spectra of recorded earthquake ground motion using wavelets. J Earthq Eng 2006;10(1):67–89. [special issue].
[43] Hancock J, Bommer JJ, Stafford PJ. Numbers of scaled and matched accelerograms required for inelastic dynamic analyses. Earthq Eng Struct Dyn 2008;37:1585–607.
[44] American Association of State Highway and Transportation Officials (AASHTO). Guide specifications for LRFD seismic bridge design. 1st ed. Washington (DC): AASHTO; 2009.
[45] Ocel J, DesRoches R, Leon RT, Hess G, Krummes R, Hayes JR, Sweeney S. Steel beam–column connections using shape memory alloys. J Struct Eng 2004;130(5):732–40.
[46] Janke L, Czaderski M, Motavalli M, Ruth J. Application of shape memory alloys in civil engineering structures – Overview, limits and new ideas. Mater Struct 2005;38(279):578–92.
[47] Deb K, Pratap A, Agrawal S, Meyarivan T. A fast elitist non-dominated sorting genetic algorithm for multi-objective optimization: NSGA-II. IEEE Trans Evolut Comput 2002;6(2):182–97.
[48] Shook D, Roschke P, Lin PY, Loh CH. GA-optimized fuzzy logic control of a large scale building for seismic loads. Eng Struct 2008;30:436–49.